Journal of Chromatography A, 1443 (2016) 233–240

Contents lists available at ScienceDirect

Journal of Chromatography A

journal homepage: www.elsevier.com/locate/chroma

Zeolitic imidazolate framework-methacrylate composite monolith characterization by inverse gas chromatography

Kareem Yusuf[a,b,*], Ahmed Yacine Badjah-Hadj-Ahmed[a,b], Ahmad Aqel[a,b], Taieb Aouak[a], Zeid Abdullah ALOthman[a,b]

[a] Department of Chemistry, College of Science, King Saud University, P.O. Box 2455, Riyadh 11451, Saudi Arabia
[b] Advanced Materials Research Chair, Department of Chemistry, College of Science, King Saud University, P.O. Box 2455, Riyadh 11451, Saudi Arabia

ARTICLE INFO

Article history:
Received 27 January 2016
Received in revised form 2 March 2016
Accepted 10 March 2016
Available online 14 March 2016

Keywords:
Metal organic framework
Zeolitic imidazolate framework
Composite material
Methacrylate monolith
Inverse gas chromatography

ABSTRACT

Thermodynamic characterization of butyl methacrylate-*co*-ethylene dimethacrylate neat monolith and zeolitic imidazolate framework-8 incorporated with butyl methacrylate-*co*-ethylene dimethacrylate composite monolith were studied using inverse gas chromatography at infinite dilution under 1 MPa column pressure and various column temperatures. The free energy of adsorption (ΔG_A), enthalpy of adsorption (ΔH_A) and entropy of adsorption (ΔS_A) were determined using a series of *n*-alkanes. The dispersive component of surface energy (γ_S^D) was estimated by Dorris-Gray and Schultz et al. methods. The composite monolith showed a more energetic surface than the neat monolith. The acidic, K_A, and basic, K_D, parameters for both materials were estimated using a group of polar probes. A basic character was concluded with more basic behavior for the neat monolith. Flory-Huggins parameter, χ, was taken as a measure of miscibility between the probes with the low molecular weight and the high molecular weight monolith. Inverse gas chromatography provides a better understanding of the role of incorporated zeolitic imidazolate framework (ZIF-8) into the polymer matrix in its monolithic form.

1. Introduction

Materials characterization using inverse gas chromatography [IGC] is a well-known technique to investigate the thermodynamic properties of various solid materials [1–6]. In contrast to conventional chromatographic techniques, IGC is turned to stationary phase characterization by observing the behavior of standard solutes injected over a temperature range; as a result, the term "inverse" is typically used. The method is simple, inexpensive, accurate and rapid. The physicochemical characterization of polymers is the most widely used application of IGC; however, the majority of IGC studies examined linear polymers rather than crosslinked [7–12].

Monolithic stationary phases were first introduced approximately five decades ago for gas chromatographic applications [13]; however, the use of monolithic columns in GC is still very limited [14–16] compared to the enormous development of monoliths for LC applications [17]. Basically, monolithic stationary phases are of two main types, inorganic silicates and organic polymers formed as a one piece material of a continuous interconnected network of pores [18]. Inorganic silica-based monoliths are known to have the advantage of separating small molecules, in contrast to organic monoliths, which were originally designed to separate macromolecules. The introduction of a nano- or micro-particles within the polymeric mixture to form a monolithic composite stationary phase is a successful trend to enhance the separation ability of organic monoliths toward small molecules; for this purpose, various particles were tested [19–30].

Metal-organic frameworks (MOFs) of micro- and nano-particles comprise one of the most interesting materials incorporated with monoliths [17,31]. The unique properties of MOF materials provided the monolithic matrix with a further high surface area, micro- and nano-pores, as well as a specific chemical nature, including chiral selectors. MOFs are highly ordered crystalline porous materials with superior properties concerning their high surface area, chemical and physical stability, unlimited diversity and easy manipulation through the precise selection of its primary precursors and preparation conditions [32].

Recently, our research group published the first contribution of MOF-monolith composite in gas chromatography [29]. The effect

* Corresponding author at: Department of Chemistry, College of Science, King Saud University, P.O. Box 2455, Riyadh 11451, Saudi Arabia.
E-mail addresses: dr_kareemyusuf@yahoo.com, kmahmoud@ksu.edu.sa (K. Yusuf), ybadjah@ksu.edu.sa (A.Y. Badjah-Hadj-Ahmed), aifseisi@ksu.edu.sa (A. Aqel), taouak@yahoo.fr (T. Aouak), zaothman@ksu.edu.sa (Z.A. ALOthman).

http://dx.doi.org/10.1016/j.chroma.2016.03.025
0021-9673/

of incorporation of different percentages of zeolitic imidazolate framework-8 (ZIF-8) micro-particles into a butyl methacrylate-*co*-ethylene dimethacrylate (BuMA-*co*-EDMA) monolith has been explored and compared to a neat monolith as well as an open tubular commercial column, giving a surprisingly higher efficiency and fast separation. From a chromatographic perspective, the mentioned composite (ZIF-8–(BuMA-*co*-EDMA)) combines the advantages of both MOF high surface area and monolithic matrix permeability; however, such columns require more in-depth studies. In the current work, we performed an extensive IGC study of a ZIF-8–(BuMA-*co*-EDMA) composite column to achieve a deeper understanding of its superiority.

Inverse gas chromatographic studies for monoliths in their crosslinked monolithic form are very rare [33,34]. The weight, morphology, heterogeneity and defects of stationary phases were reported to have an obvious effect on its thermodynamic properties [35,36]. Thus, performing IGC studies using the monolithic columns instead of using a packed column with the grinded material has a relative advantage. The Kurganov group investigated the effect of different degrees of crosslinking in methacrylate and styrene based monolithic columns by means of IGC [33]. They used gaseous light alkanes for the study (ethane, propane, and *n*-butane) and a modified gas chromatograph for high-pressure separation (up to 10 MPa). The enthalpy-entropy compensation effect was discussed in another publication by the same research group for three monoliths with different polarities and for five different carrier gases under high pressure [34]. The hydrophilic monolith based on a methacrylate polymer showed a stronger interaction toward the light hydrocarbons than the hydrophobic monolith. They also concluded that the high-pressure separation has no strong effect on the separation process.

The present work is considered as complementary research to the previously published work on the zeolitic imidazolate framework-8-butyl methacrylate-*co*-ethylene dimethacrylate composite monolith for GC applications. Butyl methacrylate-*co*-ethylene dimethacrylate (neat monolith) and ZIF-8-butyl methacrylate-*co*-ethylene dimethacrylate (composite monolith) monoliths were prepared and investigated via a classical low-pressure gas chromatograph. At infinite dilution, a series of linear alkanes (pentane, hexane, heptane, octane, and nonane), alkylbenzenes (benzene, toluene, ethylbenzene, propylbenzene, and butyl benzene), and a group of polar probes, (diethyl ether (DEE), acetone (Acet.), dichloromethane (DCM), tetrahydrofuran (THF), chloroform (CHL), and ethyl acetate (EtAc.)) have been utilized to calculate various thermodynamic parameters. The free energy of adsorption (ΔG_A), enthalpy of adsorption (ΔH_A), entropy of adsorption (ΔS_A), dispersive component of surface energy (γ_S^D), acid-base characteristics and Flory-Huggins (χ) parameters were determined at constant pressure (1 MPa) over a temperature range of 110–150 °C.

2. Experimental

2.1. Reagents and materials

Basolite®Z1200 [2-methylimidazole zinc salt (ZIF-8)] was obtained from Sigma-Aldrich (St. Louis, MO, USA). Fused silica capillaries with internal diameter of 250 μm were purchased from Restek (Bellefonte, USA). The initiator azobisisobutyronitrile (AIBN) and the spacer 3-(trimethoxysilyl) propyl methacrylate (TMSM) were obtained from Fluka (Buchs, Switzerland). The monomer Butyl methacrylate (BuMA) and the crosslinker ethylene dimethacrylate (EDMA) were purchased from Sigma-Aldrich (St. Louis, MO, USA). High-purity grade (99.9999%) gases (air, helium, hydrogen, nitrogen and methane), were purchased from SIGAS (Riyadh, Saudi Arabia). *n*-Alkanes (pentane, hexane, heptane, octane, and nonane), alkylbenzenes (benzene, toluene, ethylbenzene, propylbenzene, and butylbenzene) as well as polar probes (diethyl ether, dichloromethane, tetrahydrofuran, chloroform, and ethyl acetate) all of the highest purity grade, were obtained from Merck (Darmstad, Germany).

2.2. Instrumentation

All GC separations were performed on a conventional chromatographic system (Trace GC Ultra, Thermo Scientific, USA) consisting of split/splitless injector, an oven with a temperature range of 50–400 °C and a flame ionization detector (FID). All the experiments were performed at constant pressure (1 MPa) and over a temperature range of 110–150 °C. Both the injector and the detector were adjusted to 190 °C. The carrier gas was dry, high-purity helium. Data acquisition and processing were performed using the Chrom-Card data handling software package.

2.3. Preparation of monolithic capillary columns

Two batches of columns were prepared to examine the effect of adding ZIF-8 on the thermodynamic properties of the monolith; one batch contains only the neat (BuMA-*co*-EDMA) monolith, and the other batch was loaded with a composite monolith containing 10 mg mL^{-1} of ZIF-8 [29]. The polymerization mixture consisting of 21% BuMA, 9% EDMA, 35% 1-propanol and 35% 1,4-butandiol. ZIF-8 was dispersed and homogenized in the polymerization mixture and then purged with nitrogen for 5 min. The empty fused silica capillaries (250 μm i.d) were activated and modified with 10% 3-(trimethoxysilyl) propyl methacrylate (TMSM) in toluene solution for 10 min, as described in a previous work [16]. After activation, 33.5 cm long × 250 μm i.d. empty capillaries were filled with the polymerization mixture and then thermally polymerized using AIBN as an initiator at 60 °C for 16 h. Finally, the prepared columns washed with acetonitrile over night to remove the unreacted materials and porogenic solvents.

2.4. Inverse gas chromatography (IGC)

At infinite dilution (zero surface coverage), where the adsorbate-adsorbate interactions could be neglected and Henry's law is obeyed, the net retention volume, V_N (Table S1), is the fundamental parameter that is directly linked to the thermodynamic interactions with the studied surfaces. In these conditions the net retention volume is expressed by Eq. (1) [1]:

$$V_N = (t_R - t_M)\, F_a \frac{T}{Ta} J \tag{1}$$

where t_R is the retention time (Table S2), t_M is the dead time (determined experimentally using methane), F_a is the volumetric flow rate ($cm^3\ min^{-1}$) determined practically using bubble flowmeter, T and T_a are the column temperature (K) and the ambient temperature (K) respectively and J is the James-Martin gas compressibility correction factor that elucidates the pressure drop along the chromatographic column [37] and is determined according to the following Eq. (2):

$$J = \frac{3\left(P^2 - 1\right)}{2\left(P^3 - 1\right)} \tag{2}$$

with P being P_i/P_o, Where P_i is the inlet pressure (at the column pressure), and P_o is the outlet pressure (at atmospheric pressure).

The specific retention volumes, V_g (Table S3), is calculated from the net retention volume, Eq. (3) [38]:

$$V_g = \frac{V_N 273.15}{wT} \tag{3}$$

where w is the weight of the stationary phase.

The free energy of adsorption, ΔG_A, (Table S4) is related to V_g as follows, Eq. (4) [39]:

$$\Delta G_A = -RT\ln\left(\frac{V_g P^o}{S\pi_0}\right) \quad (4)$$

where R is the ideal gas constant, S is the specific surface area of adsorbent, π_0 is the reference two-dimensional surface pressure (whose standard state is arbitrary and was taken as $\pi_0 = 0.338\ mJ/m^2$ proposed by de Boer [40]), and P° is the adsorbate vapor pressure in the gaseous standard state (Table S5), which calculated from the Antoine's equation, Eq. (5):

$$\log\left(P^\circ\right) = A - \left(\frac{B}{t+C}\right) \quad (5)$$

where A, B and C are the Antoine coefficients (Table S6), and t is the column temperature in Celsius.

The enthalpy of adsorption, ΔH_A, is calculated from Eq. (6) and the slope of straight line indicating the variation of $\ln V_g$ versus 1/T (Figs. S1–S4):

$$\Delta H_A = -R\frac{d\ln V_g}{d\left(1/T\right)} \quad (6)$$

The entropy of adsorption, ΔS_A, is evaluated from ΔG_A and ΔH_A values using Eq. (7):

$$\Delta S_A = \frac{\Delta H_A - \Delta G_A}{T} \quad (7)$$

The dispersive component of surface energy, γ_S^D, is a common parameter that measures the energetic activity of the solid's surface and is considered as the analog of surface tension in liquids [41]. For the estimation of the dispersive interactions between the mobile and the solid phase, two different methods have been described: one by Dorris–Gray [42], and the other by Schultz et al. [43]. Dorris-Gray [42] suggested a relation to evaluate γ_S^D (Figs. S5 and S6) based on Fowkes's approach [41] concerning the solid stationary phase and methylene group adhesion, Eq. (8):

$$\gamma_S^D = \frac{1}{4\gamma_{CH2}}\left(\frac{RT\frac{V_{N,n+1}}{V_{N,n}}}{Na_{CH2}}\right)^2 \quad (8)$$

where N is Avogadro's number, a_{CH2} ($\approx 6\ Å^2$) is the cross-sectional area of an adsorbed methylene group. $V_{N,n+1}$ and $V_{N,n}$ are the net retention volumes of *n*-alkanes with carbon number n + 1 and n, respectively, γ_{CH2} (mJ/mol) is the surface dispersive free energy of solid material containing only methylene groups and is calculated at various temperatures, t (°C), using Eq. (9):

$$\gamma_{CH_2} = 35.6 - 0.058t \quad (9)$$

Schultz et al. [43] has studied the work of adhesion between the solid stationary phase and the solute probe according to the Fowke's approach. They derived a relation between the surface dispersive free energy and the net retention volume (Figs. S7 and S8), Eq. (10):

$$RT\ln V_N = 2Na(\gamma_L^D.\gamma_S^D)^{1/2} + K \quad (10)$$

where a is the cross-sectional area, and γ_L^D is the dispersive free energy of the solute probe (Table 1). γ_S^D is evaluated from the slope of the linear relation between RT. $\ln V_N$ and $a\left(\gamma_L^D\right)^{1/2}$.

For polar probes, the specific interactions occur together with the dispersive interactions. The acid-base surface interactions represent the majority of the specific interactions in absence of electrostatic, metallic, or magnetic interactions [6]. The free energy of adsorption for polar probes, ΔG_A, is the sum of dispersive and specific free energy of adsorption (ΔG^D and ΔG^{SP}, respectively) [44,45], Eq. (11):

$$\Delta G_A = \Delta G^D + \Delta G^{SP} \quad (11)$$

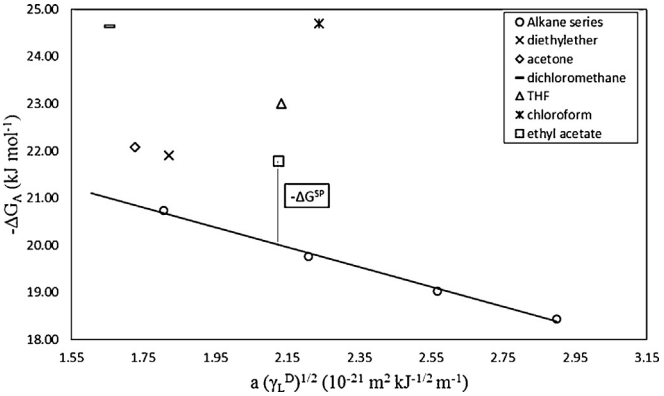

Fig. 1. The application of Schultz et al. method to calculate ΔG^{SP} for polar probes (diethylether, acetone, dichloromethane, tetrahydrofuran, chloroform, ethyl acetate) on neat monolith at 110 °C.

In this work, we used the method of Schultz et al. to determine the specific free energy of adsorption [46] by plotting $-\Delta G_A$ as a function of a $\left(\gamma_L^D\right)^{1/2}$ of polar probes at the studied temperature range (Figs. S9–S18). ΔG^{SP} is represented by the vertical distance between the free energy of adsorption of polar probes and the free energy of adsorption of hypothetical alkane on the *n*-alkane reference line (Fig. 1), Eq. (12):

$$\Delta G^{SP} = \Delta G_{polar} - \Delta G_{ref} \quad (12)$$

The specific component of enthalpy of adsorption of the polar probes, ΔH^{SP}, was estimated directly from the slope of $\Delta G^{SP}/T$ versus the reverse of temperature.

The acceptor and the donor constants, K_A and K_D respectively, which describe the acidity and the basicity of the examined stationary phase are calculated from the following Eq. (13):

$$\frac{\Delta H^{sp}}{AN^*} = \frac{DN}{AN^*}K_A + K_D \quad (13)$$

where AN* (kJ/mol) is the modified acceptor number of Riddle and Fowkes [47], and DN (kJ/mol) is Gutmann's donor number [48]. The slope of the linear relation between $-\Delta H^{sp}/AN^*$ versus DN/AN^* represents the value of K_A, and the intercept corresponds to K_D.

The Flory-Huggins interaction parameter (χ) reflects the polymer (used as solvent)-probes (used as solute) miscibility. Assuming that the effect of the incorporated ZIF-8 particles in the composite monoliths is neglected due to its low contribution (≈1%). At infinite dilution of the probes and for high molecular weight of the stationary phase, the Flory-Huggins interaction parameter can be estimated from Eq. (14):

$$\chi_{12}^{\infty} = \ln\left(\frac{273.15R\upsilon_2}{p_1^\circ V_g V_1^\circ}\right) - \frac{p_1^\circ}{RT}\left(B_{11} - V_1^\circ\right) - 1 \quad (14)$$

p_1° is the saturated vapor pressure of the solute at column temperature, B_{11} is the second virial coefficient of the solute (Table S7), V_1° is the molar volume (Table S8) and υ_2 is the specific volume of the polymer.

The second virial coefficient, B_{11}, could be determined by using various methods. According to Guggenheim and McGlashan [49] this coefficient is expressed by the following relationship:

$$\frac{B_{11}}{V^c} = 0.461 - 1.158\left(\frac{T^c}{T}\right) - 0.503\left(\frac{T^c}{T}\right)^3 \quad (15)$$

Table 1
Characteristics of *n*-alkanes (pentane, hexane, heptane, octane and nonane) and polar probes (diethylether, acetone, dichloromethane, tetrahydrofuran, chloroform and ethylacetate) used in this work [62–64].

Probe	a (Å)^2	γ_L^D(mJ m^2)	DN (kJ mol^{-1})	AN* (kJ mol^{-1})	Specific characteristic
Pentane	45.00	16.10	0	0	Neutral
Hexane	51.50	18.40	0	0	Neutral
Heptane	57.00	20.30	0	0	Neutral
Octane	62.80	21.30	0	0	Neutral
Nonane	68.90	22.70	0	0	Neutral
Diethylether	47.00	15.00	80.33	5.86	Basic
Acetone	42.50	16.50	71.13	10.46	Basic
Dichloromethane	31.50	27.60	0	16.30	Acidic
THF	45.00	22.50	83.68	2.09	Basic
Chloroform	44.00	25.90	0	22.59	Acidic
Ethylacetate	48.00	19.60	71.55	6.28	Basic

a: surface area of the probe molecule, γ_L^D : dispersive component of the surface energy of the probe, DN: Gutman's electron donor number, AN*: Riddle-Fowkes' electron acceptor number.

where T and T^c are the column and critical temperatures (Table S8), and V^c is the critical volume.

3. Results and discussion

3.1. Thermodynamics of adsorption

At infinite dilution, the retention time of all analytes decreased as a function of column temperature, either for a neat or a composite monolith, indicating exothermic separation. Van't Hoff plots of selected probes (Fig. 2) show a good linear correlation between ln k (retention factor) and 1/T, suggesting no change in the separation mechanism over the working temperature range. The specific retention volume, V_g, values are directly proportional to the probe chain length due to the decrease of vapor pressure with probe chain length [50]. The morphology of the studied stationary phase has a strong influence on specific retention volume as well as its chemical nature; therefore, the effect of monolithic structure on V_g should differ from that of a particulate polymer and, by extension, on all thermodynamic parameters [35]. The free energy change of adsorption, ΔG_A, is the sum of the energies of adsorption attributable to the dispersive and specific interactions. The adsorption of *n*-alkanes as nonpolar probes occurs through dispersive interactions only, whereas for polar probes, both London and acid-base interactions contribute to ΔG_A, as we will see later [51]. Negative values of ΔG_A (Table S4) indicate a spontaneous process of solutes transfer from mobile phase to stationary phase for both columns.

The physical and chemical adsorption are typically distinguished on the basis of the enthalpy change of adsorption (ΔH_A), with a typical value of 62.8 kJ/mol that corresponds to an arbitrary dividing line between physical and chemical adsorption [52]. Table 2 shows that the values of the enthalpy change of adsorption for neat and composite columns do not exceed the limit between physical and chemical adsorption, indicating only physical interactions for alkanes. The composite column exhibits higher absolute values of the enthalpy change of adsorption, corresponding to greater interaction between adsorbate and adsorbent. The chain length effect of the *n*-alkanes and *n*-alkylbenzenes series on the enthalpy of adsorption exhibits a linear relation for both columns (Fig. 3) due to the additive nature of dispersive interaction [36]. The comparison between the heat of liquefaction for *n*-alkanes (*n*-hexane: 31.7 kJ/mol, *n*-heptane: 36.9 kJ/mol, *n*-octane: 41.8 kJ/mol, *n*-nonane: 46.8 kJ/mol) [53] and its enthalpy change of adsorption on both columns demonstrated that the interactions across the interface monolith- *n*-alkanes arise from the secondary weak intermolecular forces or Liftshitz—van der Waals forces, as these values are very close to each other [50]. Both the enthalpy of adsorption ΔH_A and the entropy of adsorption ΔS_A increase with an increase in the probe chain length for the *n*-alkanes series (Table 2), in

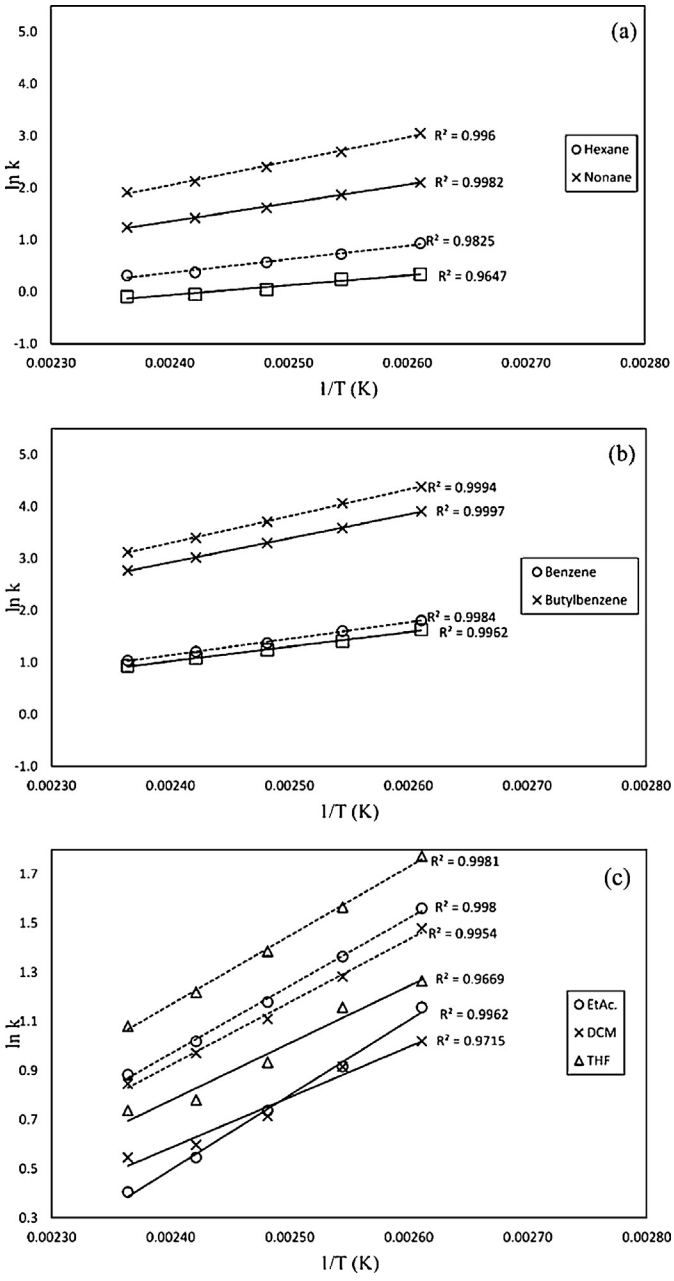

Fig. 2. Van't Hoff plots for: (a) hexane, nonane, (b) benzene, butyl benzene and (c) ethylacetate, dichloromethane, tetrahydrofuran: (—) neat monolith, (-----) composite monolith.

Table 2
ΔH_A and ΔS_A values of *n*-alkanes (hexane, heptane, octane and nonane) on neat monolith and composite monolith.

Alkanes	ΔH_A (kJ mol^{-1})		ΔS_A (J mol^{-1} K^{-1})	
	Neat	Composite	Neat	Composite
Hexane	−24.64	−30.52	−9.05	−34.14
Heptane	−29.51	−35.94	−23.18	−48.69
Octane	−34.00	−41.80	−35.98	−64.18
Nonane	−38.40	−47.31	−48.47	−78.54

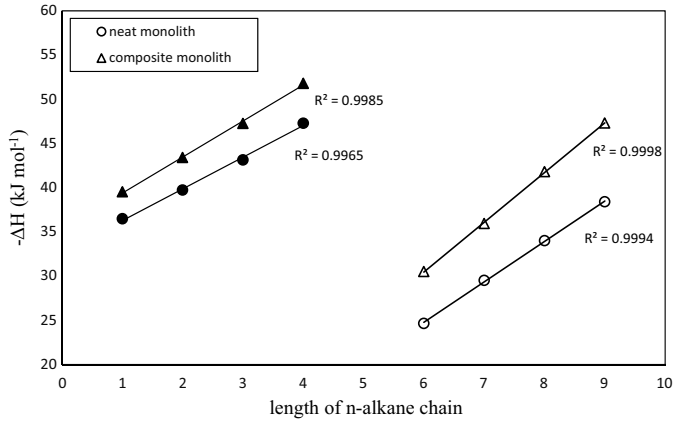

Fig. 3. Effects of the alkyl chain length on ΔH_A for *n*-alkanes (open markers) and *n*-alkylbenzenes (solid markers) in both the neat monolith and the composite monolith.

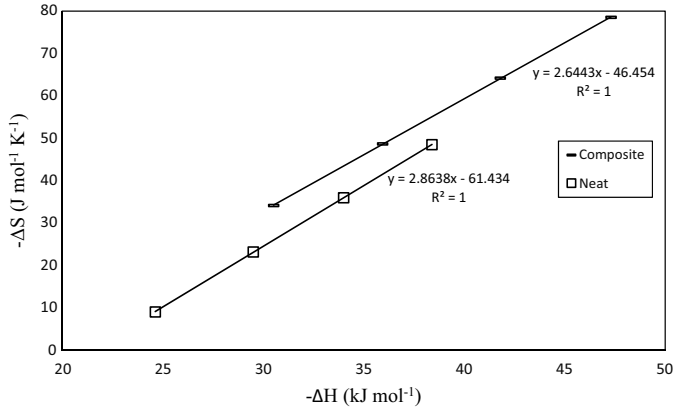

Fig. 4. The correlation between entropy of adsorption, ΔS_A, and enthalpy of adsorption, ΔH_A, of alkanes (hexane, heptane, octane and nonane) on neat monolith and composite monolith.

agreement with a previous study on polymeric monoliths [34]. A large entropy change of adsorption indicated that the adsorbate molecules are more retained with less random movement along the column [54]. The composite monolith showed a less random adsorption system with larger ΔS_A values than the neat monolith, revealing a larger capability for separating smaller molecules with high efficiency.

Fig. 4 shows a perfect linear correlation between $-\Delta H_A$ and $-\Delta S_A$, i.e., the "thermodynamic compensation effect" with correlation coefficient equals 1 for both monoliths, indicating a higher loss of freedom as the adsorption strength increase with *n*-alkane chain length [55]. The slopes of the linear correlation of enthalpy-entropy are called the compensation temperature T_{com}, which is almost identical for the two materials (T_{com} neat monolith: 2.86, T_{com} composite monolith: 2.64), indicating an isoequilibrium process [34]. The incorporation of ZIF-8 into butyl methacrylate-*co*-ethylene dimethacrylate monolith extended its ability toward stronger interaction with less random process.

3.2. *dispersive component γ_S^D of the surface energy*

The dispersive component of surface energy (γ_S^D) can be used to estimate the activity of a solid surface. The evaluation of surface activity of a polymer in a monolithic column form would be more accurate than the used of packed columns with the grinded polymer, as γ_S^D is affected not only by London interactions but also by the heterogeneity and defects of the material's surface [36]. The dispersive component of surface energy was estimated using both the Dorris-Gray method [42] and the Schultz et al. method [43] (Table 3). As expected, the dispersive parameters determined using the Dorris-Gray method was larger than the data determined using the Schultz method in both columns [56]. The γ_S^D values were decreased with increasing the temperature, in agreement with previous studies [57]. The γ_S^D values of the neat monolith were consistent with the same values in the literature for non-conductive polymers [58,59]. For the composite monolith, the values of γ_S^D were larger than those for the neat monolith i.e., the composite monolith has a more energetic surface than the neat monolith, which is may be due to the less polar character of the composite monolith than the neat monolith. ZIF-8 tends to have apolar character [60]; as a result, it functions as apolar functional groups that increase the values of dispersive component of surface energy [57,61].

3.3. *Acid–base characteristics*

Polar probes were used to determine the specific acid-base properties of the surfaces. Fig. 1 shows the linear relation between $[-\Delta G_A]$ of the *n*-alkanes series and their characteristic $[a(\gamma_L^D)^{1/2}]$ at 110 °C corresponding to the dispersive interactions. The free energy change of the adsorption values of polar probes lies clearly above the reference line of the *n*-alkanes, indicating the presence of non-dispersive polar interactions [62]. The difference between the ΔG_A values of polar probes and its corresponding value on the *n*-alkanes line at a given $[a(\gamma_L^D)^{1/2}]$ value equals the specific free energy of interaction (ΔG^{SP}) [63]. Generally, ΔG^{SP} values are relatively small, suggesting low specific interactions (Table 4). However, a basic behavior of both monoliths was quite obvious, as the ΔG^{SP} values of acidic probes (DCM and CHL) are larger than those of basic probes (DEE, Acet., THF, and Et.Ac.).

The very short retention time of polar probes separation (4.9–8.2 s) was the reason for the high standard deviation of ΔG^{SP} values of the neat monolith (Table 4). Therefore, the comparison between the neat and the composite monoliths through ΔG^{SP} values was not preferable. For a more complete evaluation of the specific acid-base characters, acceptor and donor interaction parameters (K_A and K_D, respectively) were calculated to define the electron donor-acceptor properties of the examined surface. K_A and K_D were calculated from the slope and the intercept, respectively, of the linear relation of $\Delta H^{SP}/AN^*$ versus DN/AN^* (Fig. 5). The K_D/K_A ratio represented the overall acid-base behavior of the surface; hence, the results of K_D/K_A ratios for both monoliths con-

Table 3
The dispersive component of surface energy γ_S^D (mJ/m^2) values using both Dorris-Gray and Schultz et al. methods for neat monolith and composite monolith at studied temperatures.

T (°C)	Neat		Composite	
	Dorris-Gray method	Schultz et al. method	Dorris-Gray method	Schultz et al. method
110	23.47	19.22	35.41	27.62
120	22.69	17.23	31.83	25.15
130	20.67	16.55	30.12	23.03
140	18.47	15.23	30.19	22.01
150	15.91	13.53	27.90	19.29

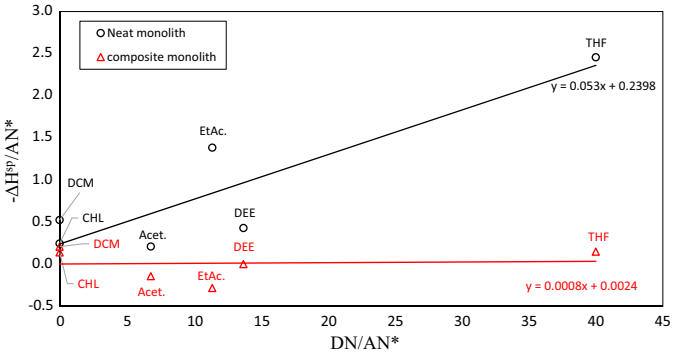

Fig. 5. The plot of $\Delta H^{SP}/AN^*$ versus DN/AN* for neat monolith and composite monolith. DEE: diethylether, Acet.: acetone, DCM: dichloromethane, THF: tetrahydrofuran, CHL: chloroform, EtAc.: ethyl acetate.

Table 4
Values of $-\Delta G^{SP}$ of the polar probes (diethylether, acetone, dichloromethane, tetrahydrofuran, chloroform and ethylacetate) on neat and composite monolith at studied temperatures.

Polar probes	$-\Delta G^{SP}$ (kJ mol^{-1})	
	Neat	Composite
Diethylether	1.35 ± 0.27	1.67 ± 0.09
Acetone	1.30 ± 0.19	1.62 ± 0.12
Dichloromethane	3.61 ± 0.22	3.98 ± 0.12
THF	2.96 ± 0.13	3.00 ± 0.15
Chloroform	4.68 ± 0.23	4.62 ± 0.07
Ethylacetate	1.42 ± 0.30	1.51 ± 0.16

firm the Lewis basic character with $K_D/K_A > 1$, but with a more basic character for the neat monolith (Table 5). The basic behavior of both monoliths was attributed to the electron donor oxygen atoms within the methacrylate polymer structure, while the presence of Lewis acidic zinc metallic center of ZIF-8 moieties in the composite monolith led to an increase its relative acidity compared to the neat monolith.

Table 5
K_A, K_D and K_D/K_A values at studied temperatures of neat monolith and composite monolith.

	Neat	Composite
K_A	0.053	0.8×10^{-3}
K_D	0.24	2.4×10^{-3}
K_D/K_A	4.5	3

3.4. Flory-Huggins interaction parameter

The Flory-Huggins interaction parameter is a reflection of the miscibility between the low-molecular-weight probe and the high-molecular-weight polymer in an inversely proportional manner. The critical value of Flory-Huggins interaction parameter is 0.5, indicating a complete miscibility between the polymer-solvent pair [64]. Table 6 shows that the interaction parameter for *n*-alkanes are higher than the critical value for both monoliths indicating poor miscibility, while the composite monolith is in better compatibility with *n*-alkanes than the neat monolith. The presence of ZIF-8 particles within the structure of the composite monolith brings more apolar character to the material [60], making it more compatible with *n*-alkanes, and as the chain length increases, the polarity decreases, and it becomes more compatible with lower Flory-Huggins parameter. In contrast, the neat monolith is relatively polar compared to the composite monolith; as a result, as the chain length increases, it becomes less compatible with a higher Flory-Huggins parameter. Alternatively, polar probes are a good solvents for both monoliths with an interaction value less than 0.5, except for acetone. Polar probes appear to be more compatible with the neat monolith than with the composite monolith due to the same polarity effect observed with *n*-alkanes. Negative values of the interaction parameter are observed for chloroform, suggesting a very strong intermolecular interaction [65].

Table 6
Flory-Huggins interaction parameters, χ_{12}^{∞}, for *n*-alkanes (hexane, heptane, octane and nonane), polar probes (diethylether, acetone, dichloromethane, tetrahydrofuran, chloroform and ethyl acetate) and benzene on neat monolith and composite monolith at studied temperatures.

Probes	χ_{12}^{∞}									
	Neat					Composite				
	150 °C	140 °C	130 °C	120 °C	110 °C	150 °C	140 °C	130 °C	120 °C	110 °C
Hexane	0.77	0.83	0.87	0.81	0.86	0.88	0.94	0.86	0.84	0.79
Heptane	0.88	0.87	0.95	0.88	0.93	0.86	0.89	0.83	0.80	0.73
Octane	0.94	0.96	0.98	0.95	0.99	0.87	0.87	0.81	0.76	0.68
Nonane	1.01	1.03	1.05	1.03	1.05	0.85	0.85	0.78	0.72	0.63
Diethylether	0.32	0.52	0.50	0.36	0.48	0.56	0.59	0.53	0.49	0.47
Acetone	0.49	0.68	0.65	0.60	0.69	0.76	0.79	0.77	0.75	0.74
Dichloromethane	0.06	0.11	0.11	0.02	0.06	0.28	0.27	0.23	0.17	0.12
THF	0.26	0.34	0.32	0.24	0.28	0.44	0.43	0.38	0.34	0.30
Chloroform	−0.12	−0.08	−0.13	−0.05	−0.22	0.05	0.03	−0.04	−0.10	−0.17
Ethylacetate	0.60	0.60	0.56	0.54	0.47	0.64	0.65	0.63	0.60	0.60
Benzene	0.30	0.28	0.27	0.26	0.20	0.49	0.45	0.42	0.34	0.32

The electron donor oxygen atoms of methacrylate polymer have strong proton-donor/proton-acceptor interaction with the proton-acceptor chloroform molecules, leading to such high compatibility. The same effect was also observed for dichloromethane, explaining the unusual retention of both compounds, despite their boiling points [29]. Benzene is considered as a good solvent for both columns; however, it is more miscible with the higher polarity neat column due to the induced dipole moment of the aromatic ring. The Flory-Huggins interaction parameter is a Gibbs free-energy parameter; consequently, it could be divided into two contributions: enthalpic component and entropic component [66]. The enthalpic component of the Flory-Huggins parameter increases with temperature, as it depends on the free volume of solvent, whereas the entropic component decreases with temperature, as it depends on the polymer-solvent intermolecular forces. Therefore, the temperature dependence of Flory-Huggins parameter could be neglected, as it may increase or decrease according to the predominant component effect [67].

4. Conclusion

MOF-polymer composite monoliths are a promising material to develop the separation ability of organic monolithic columns especially for GC applications. The current research present IGC study as a perfectly easy and precise tool to investigate the energetic behavior, acid-base characteristics as well as the miscibility parameter of ZIF-8-BuMA-*co*-EDMA composite monolith compared with the neat monolith. The presence of ZIF-8 micro-particles within the monolithic matrix extended its ability toward stronger interaction with a more energetic surface and a higher acidic apolar character. Using MOFs in monolithic column is a very new approach that needs extensive studies for better understanding of its effect and it opens a new promising arena for monolithic columns development.

Acknowledgment

The authors would like to extend their sincere appreciation to the Deanship of Scientific Research at King Saud University for its funding this Research group NO. (RGP-1437-011).

Appendix A. Supplementary data

Supplementary data associated with this article can be found, in the online version, at http://dx.doi.org/10.1016/j.chroma.2016.03.025.

References

[1] J.R. Conder, C.L. Young, Physicochemical Measurements by Gas Chromatography, Wiley, Chichester, 1979.
[2] D.R. Lloyd, T.C.H.P. Ward Schreiber, Inverse Gas Chromatography-Characterization of Polymers and Other Materials, ACS Symposium Series No. 391, American Chemical Society, Washington, DC, 1989, pp. p. 230.
[3] E. Papirer, H. Balard, Interfacial Phenomena in Chromatography, in: E. Pefferkorn (Ed.), Marcel Dekker, New York, 1999, p. 145.
[4] A. Voelkel, Inverse gas chromatography: characterization of polymers, fibers, modified silicas, and surfactants, Crit. Rev. Anal. Chem. 22 (1991) 411–439.
[5] F. Thielmann, Introduction into the characterization of porous materials by gas chromatography, J. Chromatogr. A 1037 (2004) 115–123.
[6] A. Voelkel, B. Strzemiecka, K. Adamska, K. Milczewska, Inverse gas chromatography as a source of physiochemical data, J.Chromatogr. A 1216 (2009) 1551–1566.
[7] J.-M. Braun, J.E. Guillet, Study of polymers by inverse gas chromatography, Adv. Polym. Sci. 21 (1976) 107–145.
[8] Z. Tan, G.J. Vancso, Molecular probing of polymeric microstructure and nonrandom partitioning of solvents absorbed in polymers by inverse gas chromatography, Macromolecules 30 (1997) 4665–4673.
[9] M. Pekar, Inverse gas chromatography of liquid polybutadienes, Polymer 43 (2002) 1013–1015.
[10] C. Zjao, J. Li, C. Zeng, Determination of the infinite dilution diffusion and activity coefficients of alkanes in polypropylene by inverse gas chromatography, J. Appl. Polym. Sci. 101 (2006) 1925–1930.
[11] A. Lavoie, B. Riedl, M. Bousmina, Study of interactions in poly(styrene-*co*-acrylonitrile)/poly (methyl methacrylate) (san/pmma) polymer blend by inverse gas chromatography, J. Polym. Eng. 27 (2007) 129–148.
[12] A.B. Nastasovic, A.E. Onjia, Determination of glass temperature of polymers by inverse gas chromatography, J. Chromatogr. A 1195 (2008) 1–15.
[13] R.P. Crowley, Chromatographic columns, US Patent 3,422,605 (1969).
[14] F. Svec, A.A. Kurganov, Less common applications of monoliths: III. Gas chromatography, J. Chromatogr. A 1184 (2008) 281–295.
[15] A.A. Kurganov, Monolithic column in gas chromatography, Anal. Chim. Acta 775 (2013) 25–40.
[16] K. Yusuf, A. Aqel, Z.A. ALOthman, A.Y. Badjah-Hadj-Ahmed, Preparation and characterization of alkyl methacrylate-based monolithic columns for capillary gas chromatography applications, J. Chromatogr. A 1301 (2013) 200–208.
[17] F. Svec, Y. Lv, Advances and recent trends in the field of monolithic columns for chromatography, Anal. Chem. 87 (2015) 250–273.
[18] F. Svec, T.B. Tennikova, Z. Deyl, Monolithic Materials: Preparation, Properties and Applications, Journal of Chromatography Library, Elsevier Science, Amsterdam, 2003.
[19] Y. Zhong, W. Zhou, P. Zhang, Y. Zhu, Preparation, characterization, and analytical applications of a novel polymer stationary phase with embedded or grafted carbon fibers, Talanta 82 (2010) 1439–1447.
[20] Y. Li, Y. Chen, R. Xiang, D. Ciuparu, L.D. Pfefferle, C. Horváth, J.A. Wilkins, Incorporation of single-wall carbon nanotubes into an organic polymer monolithic stationary phase for μ-HPLC and capillary electrochromatography, Anal. Chem. 77 (2005) 1398–1406.
[21] S.D. Chambers, F. Svec, J.M.J. Fréchet, Incorporation of carbon nanotubes in porous polymer monolithic capillary columns to enhance the chromatographic separation of small molecules, J. Chromatogr. A 1218 (2011) 2546–2552.
[22] A. Aqel, K. Yusuf, Z.A. ALOthman, A.Y. Badjah-Hadj-Ahmed, A.A. Alwarthan, Effect of multi-walled carbon nanotubes incorporation into benzyl methacrylate monolithic columns in capillary liquid chromatography, Analyst 137 (2012) 4309–4317.
[23] M.-M. Wang, X.-P. Yan, Fabrication of graphene oxide nano sheets incorporated monolithic column via one-step room temperature polymerization for capillary electrochromatography, Anal. Chem. 84 (2012) 39–44.
[24] S.D. Chambers, T.W. Holcombe, F. Svec, J.M.J. Fréchet, Porous polymer monoliths functionalized through copolymerization of a C60 fullerene-containing methacrylate monomer for highly efficient separations of small molecules, Anal. Chem. 83 (2011) 9478–9484.
[25] A. Aqel, K. Yusuf, Z.A. ALOthman, A.Y. Badjah-Hadj-Ahmed, Sporopollenin microparticle-based monolithic capillary columns for liquid chromatography, Chromatographia 78 (2015) 481–486.
[26] Y.-Y. Fu, C.-X. Yang, X.-P. Yan, Incorporation of metal-organic framework UiO-66 into porous polymer monoliths to enhance the liquid chromatographic separation of small molecules, Chem. Commun. 49 (2013) 7162–7164.
[27] H.Y. Huang, C.L. Lin, C.Y. Wu, Y.J. Cheng, C.H. Lin, Metal organic framework–organic polymer monolith stationary phases for capillary electrochromatography and nano-liquid chromatography, Anal. Chim. Acta 779 (2013) 96–103.
[28] S. Yang, F. Ye, Q. Lv, C. Zhang, S. Shen, S.J. Zhao, In situ synthesis of metal-organic frameworks in a porous polymer monolith as the stationary phase for capillary liquid chromatography, J. Chromatogr. A 1360 (2014) 143–149.
[29] K. Yusuf, A.Y. Badjah-Hadj-Ahmed, A. Aqel, Z.A. ALOthman, Fabrication of zeolitic imidazolate framework-8-methacrylate monolith composite capillary columns for fast gas chromatographic separation of small molecules, J. Chromatogr. A 1406 (2015) 299–306.
[30] K. Yusuf, A.Y. Badjah-Hadj-Ahmed, A. Aqel, Z.A. ALOthman, Monolithic metal-organic framework MIL-53(Al)-polymethacrylate composite column for the reversed-phase capillary liquid chromatography separation of small aromatics, J. Sep. Sci. 39 (2016) 880–888.
[31] K. Yusuf, A. Aqel, Z.A. ALOthman, Metal-organic frameworks in chromatography, J. Chromatogr. A 1348 (2014) 1–16.
[32] H. Furukawa, K.E. Cordova, M. O'Keeffe, O.M. Yaghi, The chemistry and applications of metal-organic frameworks, Science 341 (2013) 974–986.
[33] A. Kanatyeva, A. Korolev, V. Shiryaeva, T. Popova, A. Kurganov, Characterization of monolithic capillary columns using inverse gas chromatography, J. Sep. Sci. 32 (2009) 2635–2641.
[34] A. Korolev, V. Shiryaeva, T. Popova, A. Kurganov, Enthalpy–entropy compensation effect on adsorption of light hydrocarbons on monolithic stationary phases, J. Sep. Sci. 34 (2011) 2362–2369.
[35] A.B. Littlewood, Gas Chromatography, 2nd ed., Academic Press, New York, 1970.
[36] M.T. Luebbers, T. Wu, L. Shen, R.I. Masel, Trends in the adsorption of volatile organic compounds in a large-pore metal-organic framework IRMOF-1, Langmuir 26 (2010) 11319–11329.
[37] A.T. James, A.J.P. Martin, Gas-liquid partition chromatography: the separation and micro-estimation of volatile fatty acids from formic acid to dodecanoic acid, Biochem. J. 50 (1952) 679–690.

[38] A.B. Littlewood, C.S.G. Phillips, D.T. Price, The chromatography of gases and vapours. Part V. Partition analyses with columns of silicone 702 and of tritolyl phosphate, J. Chem. Soc. (1955) 1480.
[39] L. Lavielle, J. Schultz, Surface properties of carbon fibers determined by inverse gas chromatography: role of pretreatment, Langmuir 7 (1991) 978–981.
[40] E.F. Meyer, On thermodynamics of adsorption using gas-solid chromatography, J. Chem. Educ. 57 (1980) 120–124.
[41] F.M. Fowkes, Attractive forces at interfaces, Ind. Eng. Chem. Prod. Res. Dev. 56 (1964) 40–52.
[42] G.M. Dorris, D.G. Gray, Adsorption of *n*-alkanes at zero surface coverage on cellulose paper and wood fibers, J. Colloid Interface Sci. 77 (1980) 353–362.
[43] J. Schultz, L. Lavielle, C. Martin, The role of the interface in carbon fibre-epoxy composites, J. Adhes. 23 (1987) 45–60.
[44] F.M. Fowkes, M.A. Mostafa, Acid-base interactions in polymer adsorption, Ind. Eng. Chem. Prod. Res. Dev. 17 (1978) 3–7.
[45] D.K. Owens, R.E. Wendt, Estimation of the surface free energy of polymers, J. Appl. Polym. Sci. 13 (1969) 1741–1747.
[46] J. Schultz, L. Lavielle, C. Martin, Surface-properties of carbon-fibers determined by inverse gas-chromatography, J. Chem. Phys. 84 (1987) 231–237.
[47] F. Riddle, F.M. Fowkes, Spectral shifts in acid-base chemistry 1. van der Waals contributions to acceptor numbers, J. Am. Chem. Soc. 112 (1990) 3259–3264.
[48] V. Gutmann, The Donor–Acceptor Approach to Molecular Interactions, Plenum Press, New York, 1978.
[49] E.A. Guggenheim, M.L. McGlashan, Corresponding states in mixtures of slightly imperfect gases, Proc. R. Soc. A 206 (1951) 448–463.
[50] M. Kazayawoko, J.J. Balatinecz, M. Romansky, Thermodynamics of adsorption of *n*-alkanes on maleated wood fibers by inverse gas chromatography, J. Colloid Interface Sci. 190 (1997) 408–415.
[51] Y.C. Yang, P.R. Yoon, Determination of acid-base properties of silicas by inverse gas chromatography: variation with surface treatment, Mater. Trans. 48 (2007) 1955–1960.
[52] R.L. Grob, E.F. Barry, Modern Practice of Gas Chromatography, 4th ed., John Wiley & Sons Inc, Hoboken, New Jersey, 2004.
[53] S. Katz, D.G. Gray, The adsorption of hydrocarbons on cellophane: I. Zero coverage limit, J. Colloid Interface Sci. 82 (1981) 318–325.
[54] G. Henryk, Comparison of the differential isosteric adsorption enthalpies and entropies calculated from chromatographic data, J. Chromatogr. A 986 (2003) 89–99.
[55] J.F. Denayer, G.V. Baron, J.A. Martens, P.A. Jacobs, Chromatographic study of adsorption of *n*-alkanes on zeolites at high temperatures, J. Phys. Chem. B 102 (1998) 3077–3081.
[56] B. Shi, Y. Wang, L. Jia, Comparison of Dorris–Gray and Schultz methods for the calculation of surface dispersive free energy by inverse gas chromatography, J. Chromatogr. A 1218 (2011) 860–862.
[57] A. Voelke, E. Andrzejewska, R. Maga, M. Andrzejewski, Examination of surfaces of solid polymers by inverse gas chromatography: 1. Dispersive properties, Polymer 37 (3) (1996) 455–462.
[58] V.I. Bogillo, A. Voelkel, Surface properties of copolymers and terpolymers of styrene as studied by inverse gas chromatography, Polymer 36 (1995) 3503–3510.
[59] A.M. Taylor, J.F. Watts, M.L. Abel, M.M. Chehimi, Surface characterization of photocured aromatic methacrylate resins by inverse gas chromatography, Int. J. Adhes. Adhes. 15 (1995) 3–8.
[60] D. Peralta, G. Chaplais, A. Simon-Masseron, K. Barthelet, C. Chizallet, A.-A. Quoineaud, G.D. Pirngruber, Comparison of the behavior of metal-organic frameworks and zeolites for hydrocarbon separations, J. Am. Chem. Soc. 134 (2012) 8115–8126.
[61] A.B. Nastasovic, A.E. Onjia, S.K. Milonjic, S.M. Jovanovic, Surface characterization of macroporous glycidyl methacrylate based copolymers by inverse gas chromatography, Eur. Polym. J. 41 (2005) 1234–1242.
[62] B. Riedl, L.M. Matuana, Inverse Gas Chromatography of Fibers and Polymers, Encyclopedia of Surface and Colloid Science, Taylor & Francis, 2006.
[63] D.R. Lloyd, H.P. Schreiber, T. Ward, Inverse Gas Chromatography: Characterization of Polymers and Other Materials, American Chemical Society (ACS) Symposium Series, American Chemical Society Washington, D.C, 1989.
[64] J. Brandrup, E.H. Immergut, E.A. Grulke, Polymer Handbook, 4th ed., John Wiley & Sons, New York, 1999.
[65] A. Voelkel, J. Fall, The use of the Flory-Huggins interaction parameter for the characterization of vacuum distillation residue fractions of mineral oils, Chromatographia 41 (5) (1995) 414–418.
[66] M.J. E.I-Hibri, W. Cheng, P. Munk, Inverse gas chromatography 6. Thermodynamics of poly(.epsilon.-caprolactone)-polyepichlorohydrin blends, Macromolecules 21 (1988) 3458–3463.
[67] E. Díez, G. Ovejero, M.D. Romero, I. Díez, Polymer–solvent interaction parameters of SBS rubbers by inverse gas chromatography measurements, Fluid Phase Equilib. 308 (2011) 107–113.